Supporting Information for "Increasing hurricane intensification rate near the US Atlantic coast"

Karthik Balaguru[1], Gregory R. Foltz[2], L. Ruby Leung[1], Wenwei Xu[1],

Dongmin Kim[2,3], Hosmay Lopez[2] & Robert West[2,4]

[1]Pacific Northwest National Laboratory, Richland, WA, USA

[2]NOAA/Atlantic Oceanographic and Meteorological Laboratory, Miami, FL, USA

[3]Cooperative Institute for Marine and Atmospheric Studies, University of Miami, Miami, FL, USA

[4]Northern Gulf Institute, Mississippi State University, Mississippi State, MS, USA

Contents of this file

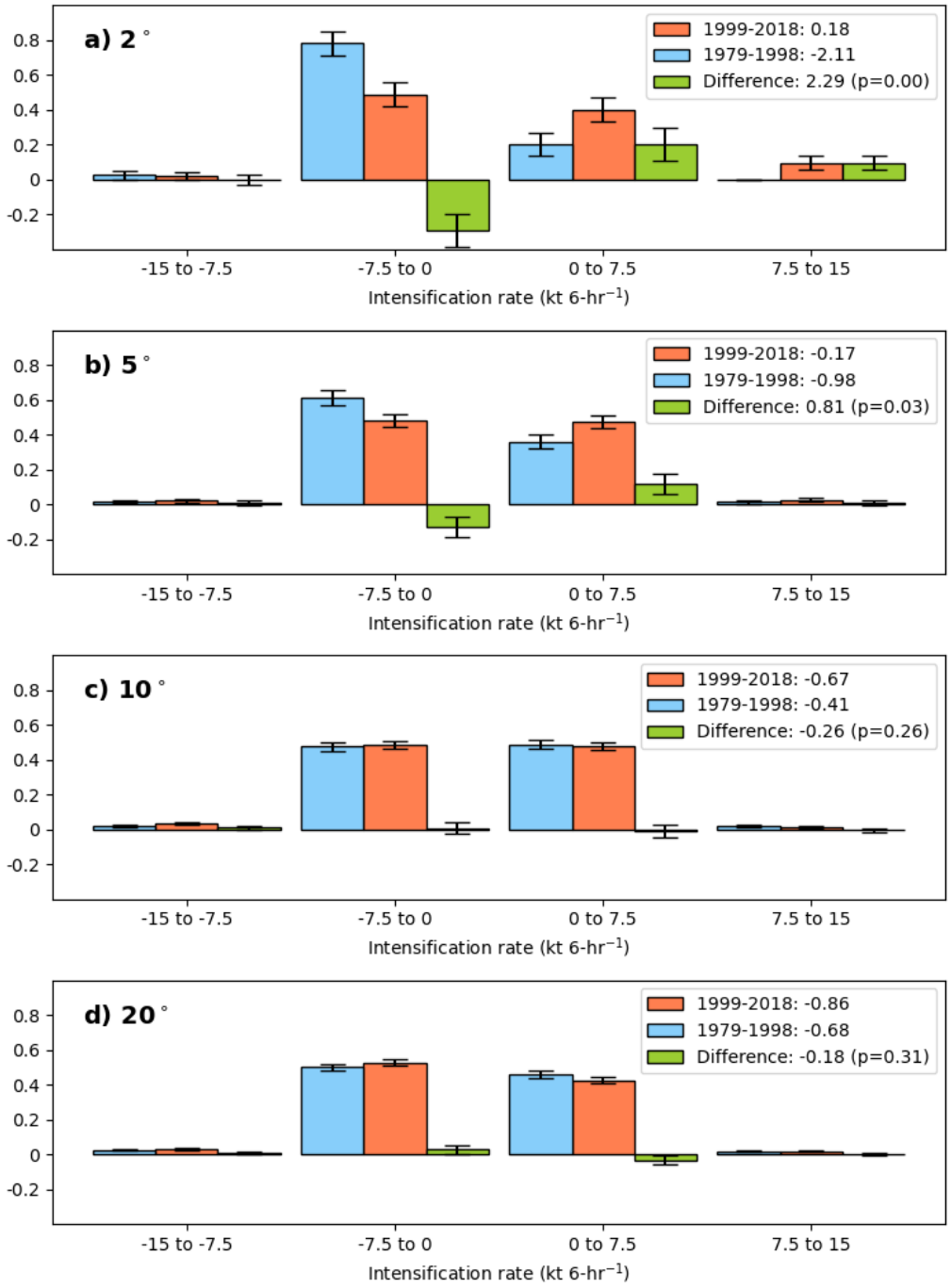

SI Figure 1. Observed changes in nearshore hurricane intensification for various distance thresholds Probability distributions of 24-hr intensification rates for the periods 1979-1998 (blue), 1999-2018 (orange) and their difference (green) based on locations that are within a) 2°, b) 5°, c) 10° and d) 20° of the US Atlantic coast. The error bars representing the standard deviation of the distribution are generated based on the Monte Carlo technique. The mean intensification rates for each period, their difference and the p-value for statistical significance (based on a Student's t-test) are shown in the legend.

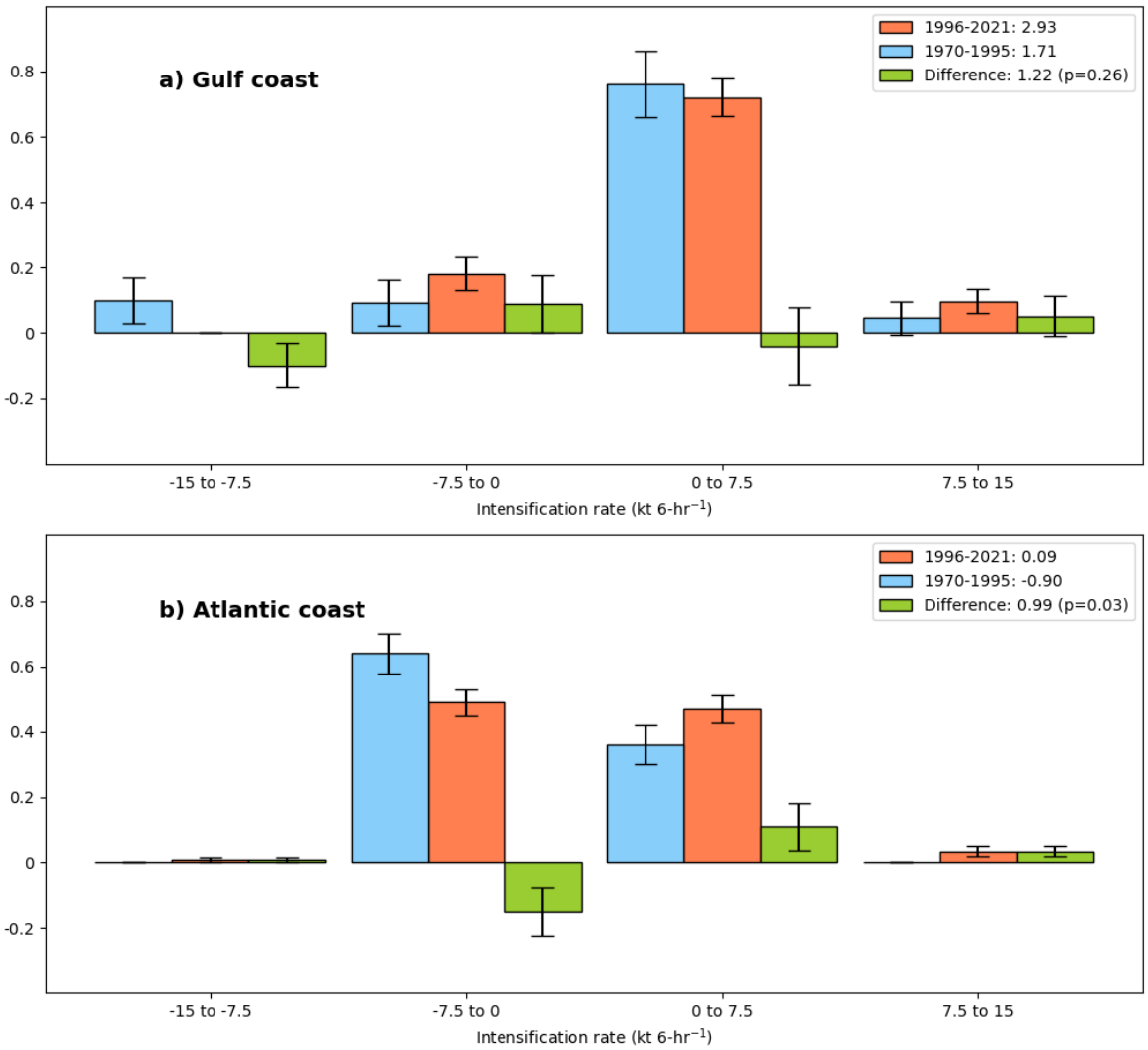

SI Figure 2. Observed changes in nearshore hurricane intensification (1970-2021) Probability distributions of 24-hr intensification rates for the periods 1970-1995 (blue), 1996-2021 (orange) and their difference (green) based on locations that are within ∼3° of the US a) Gulf and b) Atlantic coasts. The error bars representing the standard deviation of the distribution are generated based on the Monte Carlo technique. The mean intensification rates for each period, their difference and the p-value for statistical significance (based on a Student's t-test) are shown in the legend. In addition to using the translation speed thresholds described in the 'Methods' section to sub-sample data, we also consider only those locations where the initial intensity lies between 35 and 100 kt. This is to ensure that the results are not contaminated by differences in storm state between the two periods. `July 26, 2022, 10:45am`

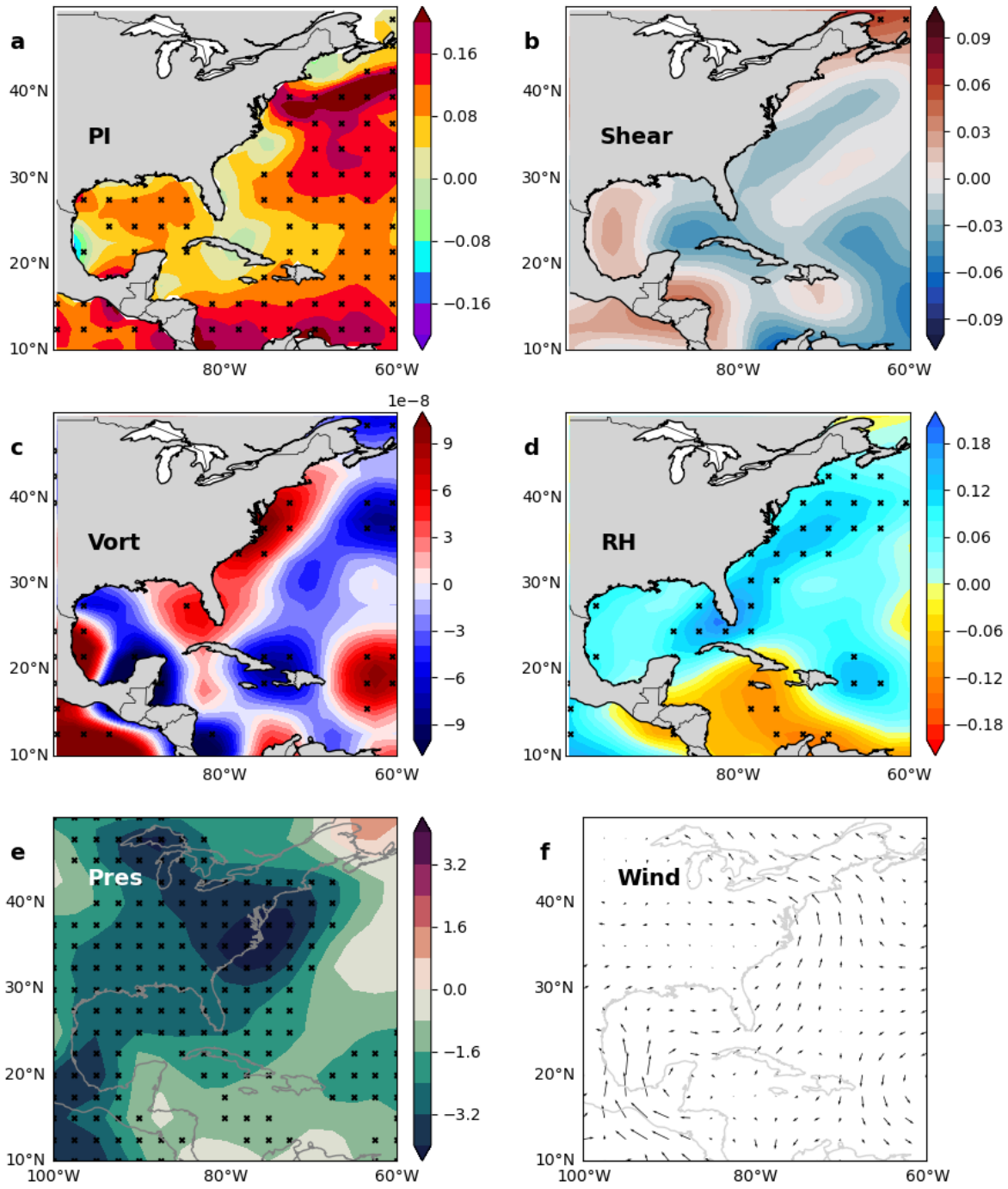

SI Figure 3. Observed changes in the nearshore hurricane environment (1979-2018) 40-year trends in a) potential intensity (ms^{-1} $year^{-1}$), b) Vertical wind shear (ms^{-1} $year^{-1}$), c) Relative vorticity at 850 hPa (s^{-1} $year^{-1}$), d) Relative humidity at 600 hPa (% $year^{-1}$), e) surface pressure (Pa $year^{-1}$), and f) circulation at 850 hPa (ms^{-1} $year^{-1}$) based on NCEP reanalysis and Hadley SST, and averaged over the months of June-October. Black crosses in various panels represent locations where the trends are statistically significant at the 95% level based on a Student's t-test.

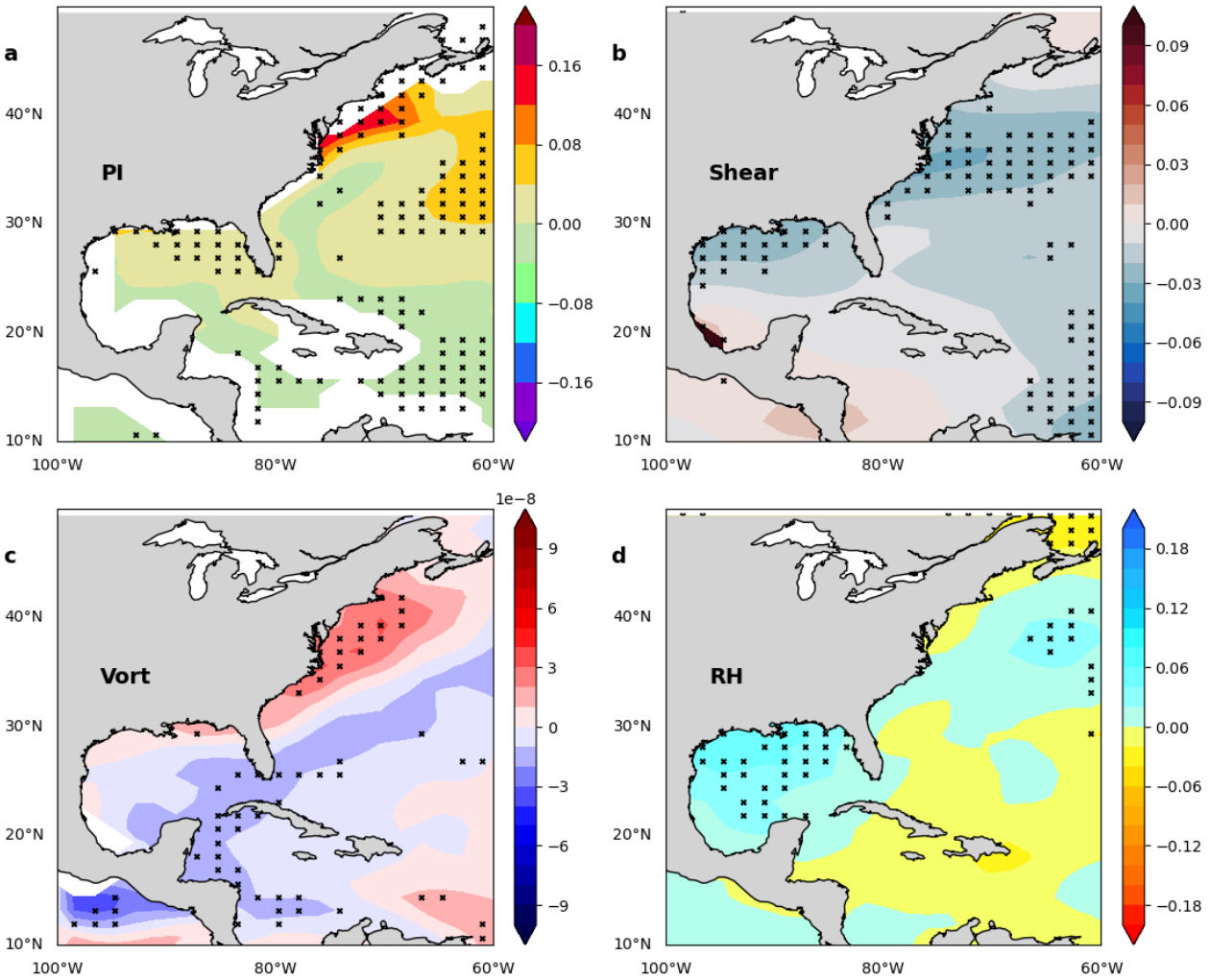

SI Figure 4. Simulated historical changes in the nearshore hurricane environment (1980-2015) Multi-model ensemble mean trends in a) potential intensity (ms^{-1} $year^{-1}$), b) vertical wind shear (ms^{-1} $year^{-1}$), c) relative vorticity at 850 hPa (s^{-1} $year^{-1}$), and d) relative humidity at 600 hPa (% $year^{-1}$), based on 15 CMIP6 climate models. Trends are computed over the 35-year historical period of 1980-2015. All parameters are averaged during June-October. Crosses represent locations where at least 11 out of the 15 models agree on the sign of the trend.

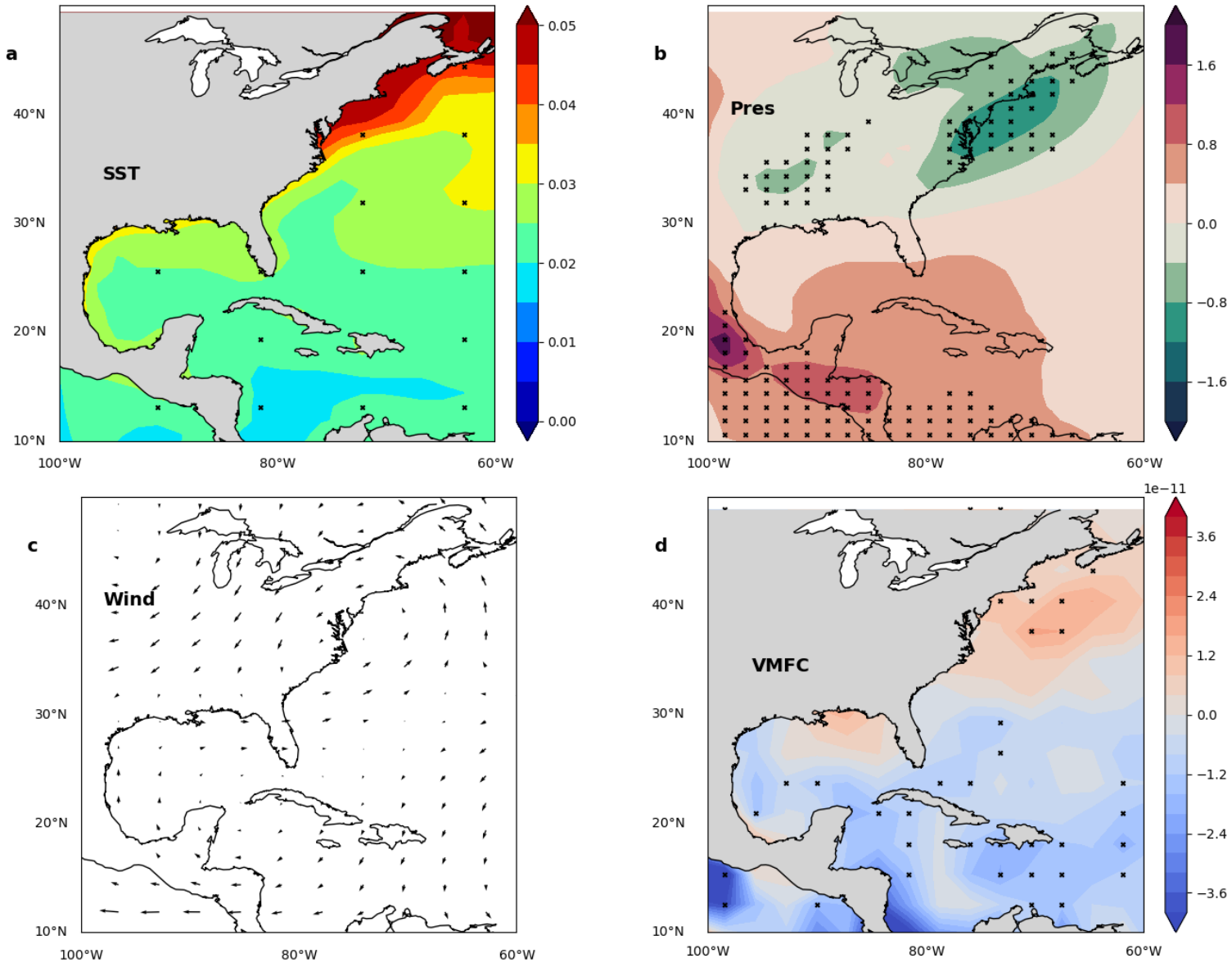

SI Figure 5. Understanding simulated historical changes in the nearshore hurricane environment (1980-2015) Multi-model ensemble mean trends in a) SST (°C year^{-1}), b) surface pressure (Pa year^{-1}), c) circulation at 850 hPa (ms^{-1} year^{-1}) and d) vertical moisture flux convergence (s^{-1} year^{-1}) at 600 hPa, based on 15 CMIP6 climate models. Trends are computed over the 35-year historical period of 1980-2015. All parameters are averaged during June-October. Crosses represent locations where at least 11 out of the 15 models agree on the sign of the trend.

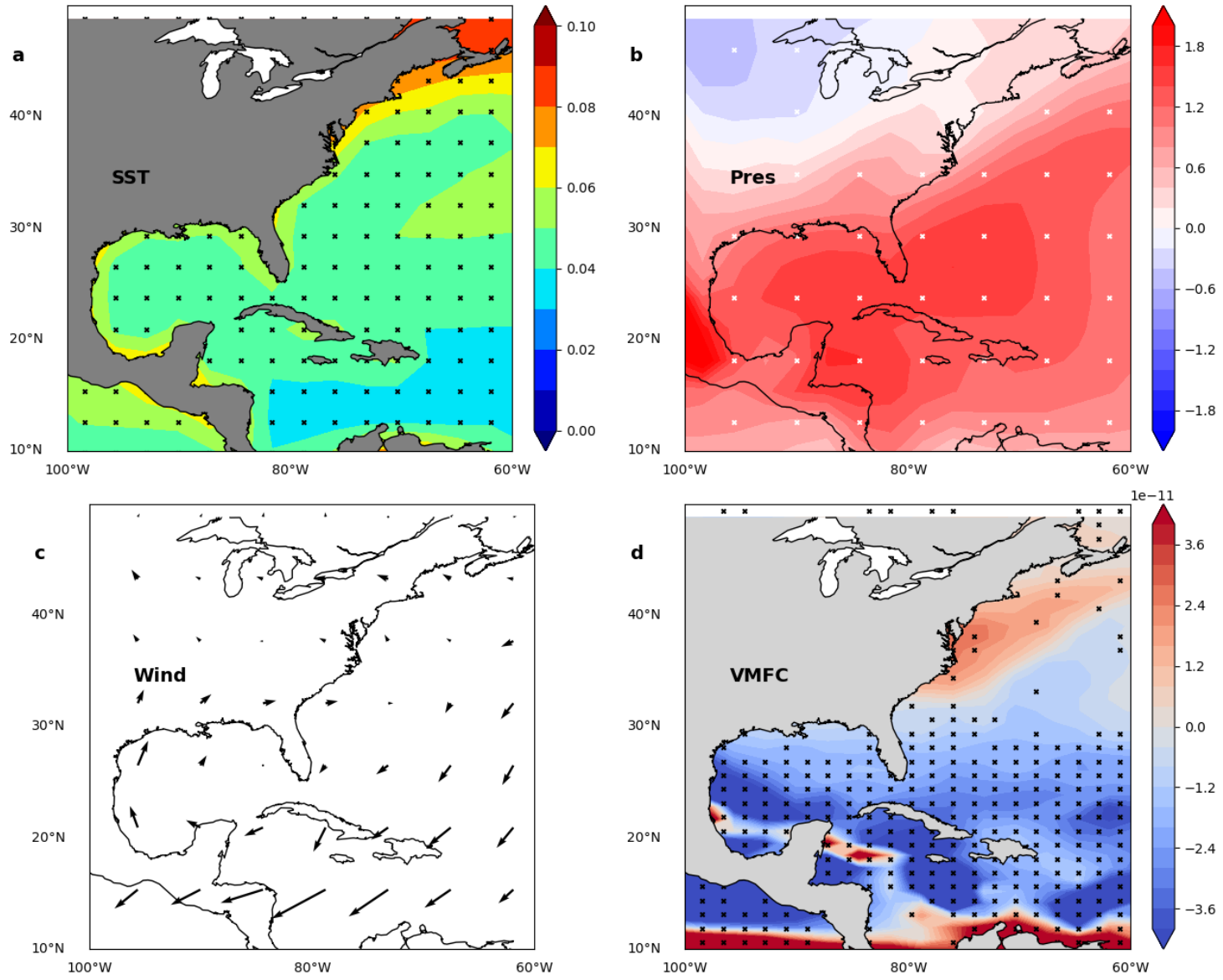

SI Figure 6. Understanding projected changes in the nearshore hurricane environment (2015-2100) Multi-model ensemble mean trends in a) SST (°C year^{-1}), b) surface pressure (Pa year^{-1}), c) circulation at 850 hPa (ms^{-1} year^{-1}) and d) vertical moisture flux convergence (s^{-1} year^{-1}) at 600 hPa, based on 15 CMIP6 climate models. Trends are computed over the 86-year period 2015-2100 based on the 'SSP585' emissions scenario. All parameters are averaged during June-October. Crosses represent locations where at least 11 out of the 15 models agree on the sign of the trend.

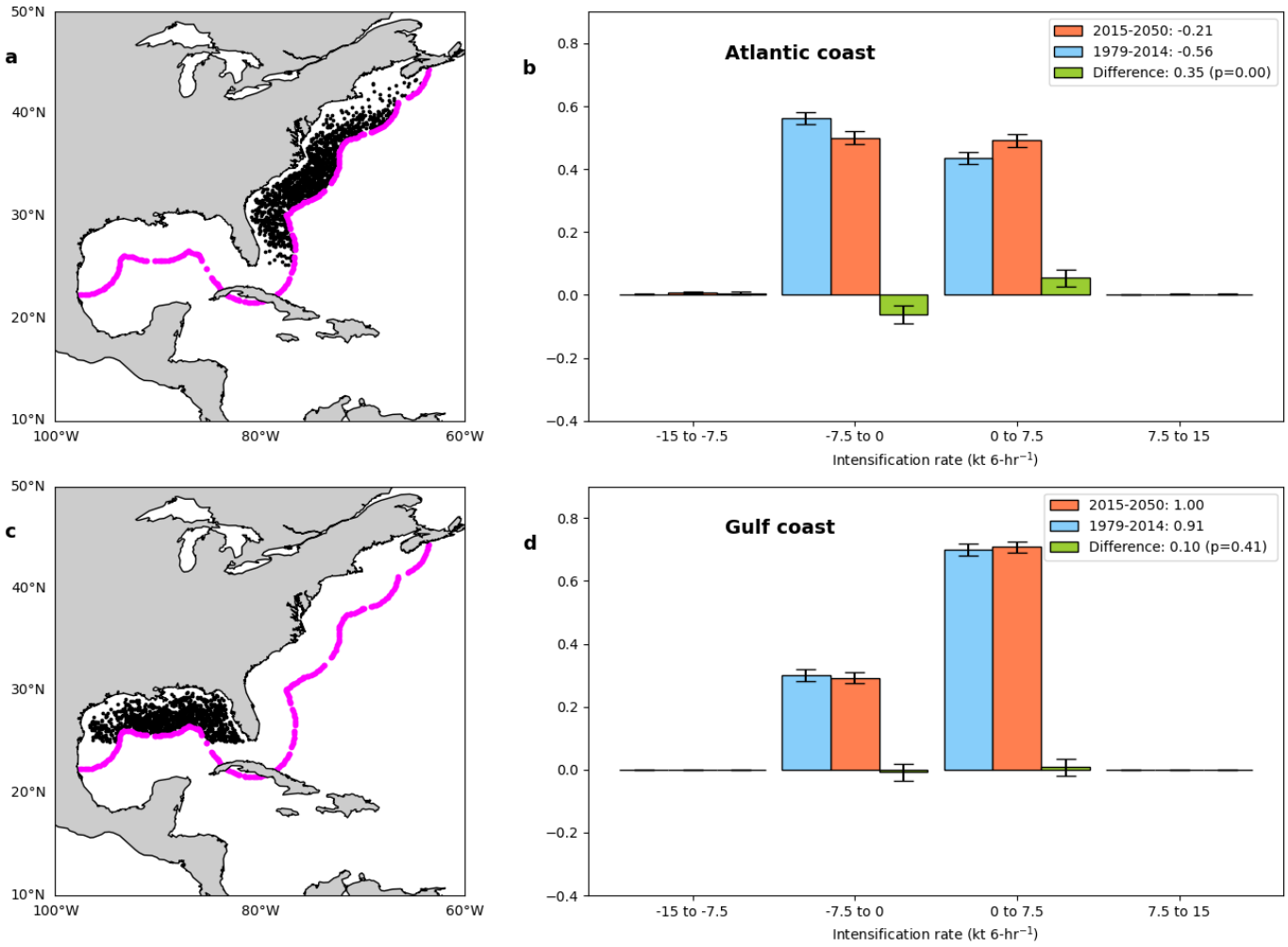

SI Figure 7. Projected changes in nearshore hurricane intensification (1979-2050) Nearshore Atlantic hurricane track locations (black dots) within ∼3° of the US a) Atlantic coast and c) Gulf coast. Probability distributions of 24-hr intensification rates for the periods 1979-2014 (blue), 2015-2050 (orange) and their difference (green) based on locations that are within ∼3° of the US b) Atlantic coast and d) Gulf coast. The error bars in panels b and d representing the standard deviation of the distribution are generated based on the Monte Carlo technique. Hurricane track data are based on 5 models belonging to HighResMIP. While data from 'hist-1950' are used for the earlier period, data from 'highres-future' are used for the future period. Track locations where the initial storm intensity is 45 kt or higher are considered for the Atlantic coast. Similarly, track locations where the initial storm intensity is between 35 and 75 kt are considered for the Gulf coast. This sub-sampling is done to ensure that the storm state is statistically similar for the two periods.

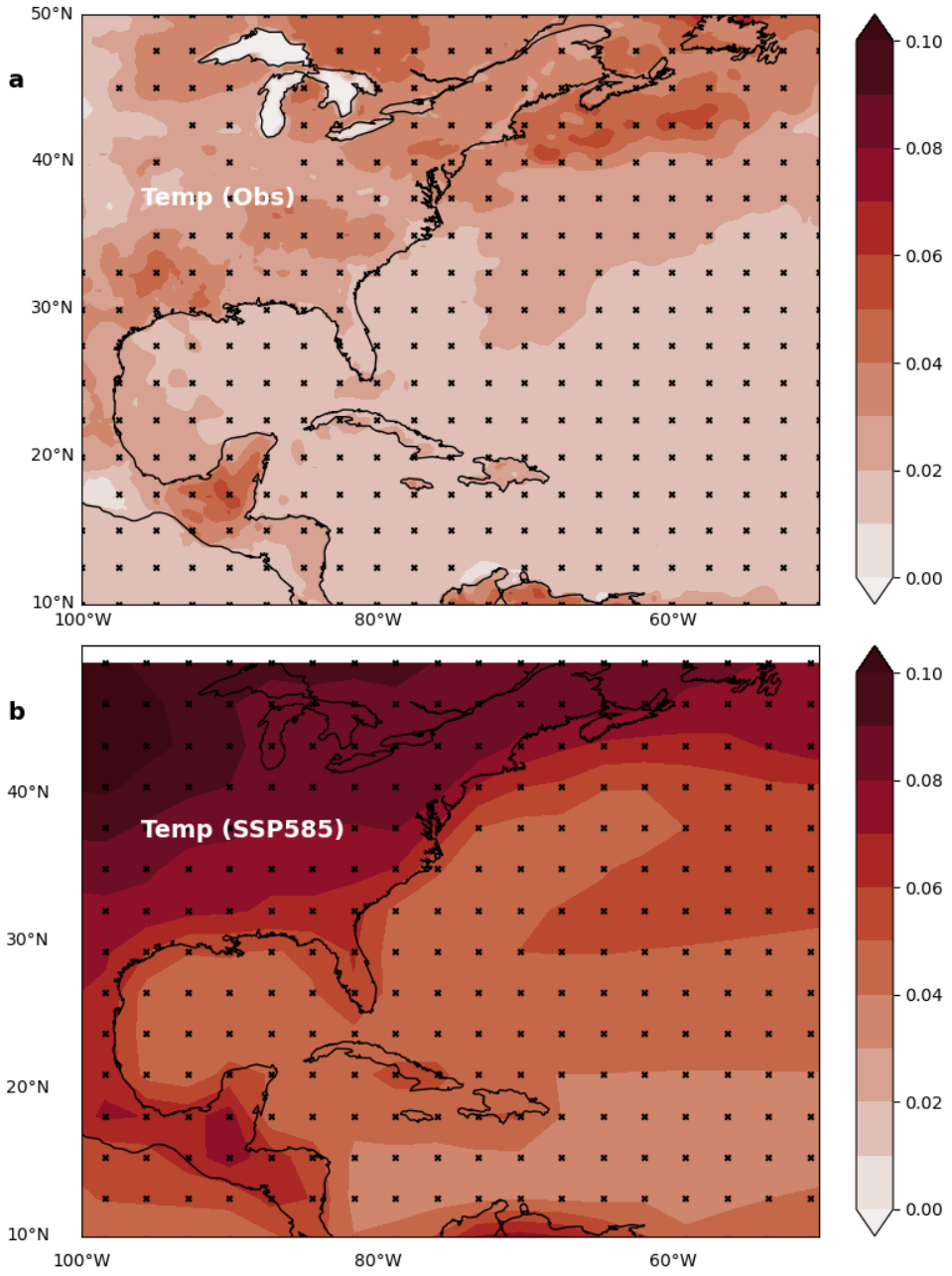

SI Figure 8. Observed and projected changes in surface temperature a) 40-year (1979-2018) trends in surface temperature (°C year^{-1}), averaged over the months of June-October, based on ERA5 reanalysis. Black crosses in various panels represent locations where the trends are statistically significant at the 95% level based on a Student's t-test. b) Multi-model ensemble mean trends in surface temperature (°C year^{-1}), averaged during June-October, based on 15 CMIP6 climate models. Trends are computed over the 86-year period 2015-2100 and based on the 'SSP585' emissions scenario. Crosses represent locations where at least 11 out of the 15 models agree on the sign of the trend.

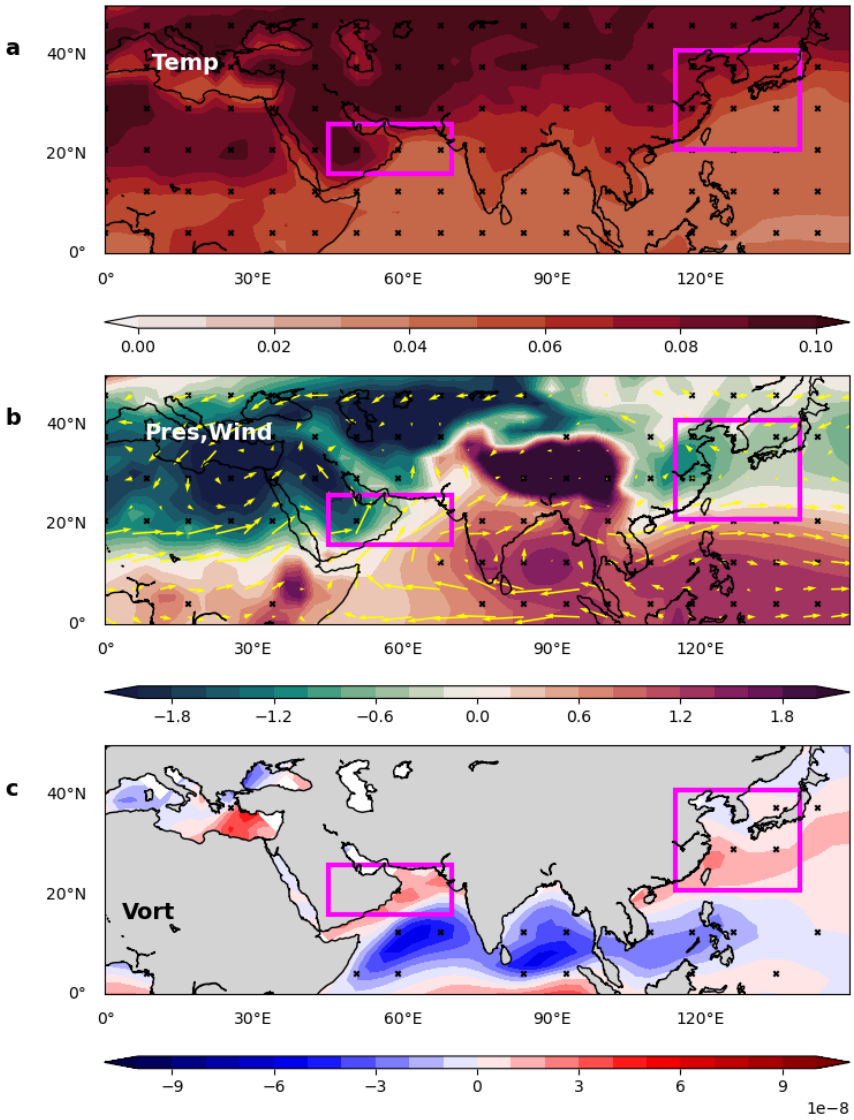

SI Figure 9. Projected future changes in the global nearshore environment Multi-model ensemble mean trends in a) surface air temperature (°C year^{-1}) , b) surface pressure (Pa year^{-1}) with vectors of 850 hPa circulation (ms^{-1} year^{-1}) overlaid and c) lower-level relative vorticity (ms^{-1} year^{-1}) based on 15 CMIP6 climate models. Trends are computed over the 86-year period 2015-2100 based on the 'SSP585' emissions scenario. All parameters are averaged during June-October. Crosses represent locations where at least 11 out of the 15 models agree on the sign of the trend. Magenta boxes enclose near-coastal regions with tropical cyclone activity where land-sea pressure gradient, cyclonic circulation and vorticity may increase significantly.

SI Table 1: List of CMIP6 models used for examining trends in the nearshore hurricane environment for the historical period (1980-2014). For each model, a single ensemble member realization from the 'historical' simulation is used.

Model (Institution)	**∼Atmospheric resolution (lat x lon)**	**Reference**
ACCESS-ESM1-5 (CSIRO-ARCCSS)	1.2° x 1.9°	Ziehn et al. (2020)
BCC-ESM1 (BCC)	2.8° x 2.8°	Wu et al. (2020)
CanESM5 (CCCma)	2.8° x 2.8°	Swart et al. (2019)
CESM2 (NCAR)	0.9° x 1.2°	Danabasoglu et al. (2020)
CNRM-ESM2-1 (CNRM-CERFACS)	1.4° x 1.4°	Séférian et al. (2019)
EC-Earth3 (EC-Earth-Consortium)	1.25° x 1.25°	Döscher et al. (2021)
E3SM-1-0 (US Dept. of Energy)	1° x 1°	Golaz et al. (2019)
GFDL-CM4 (NOAA-GFDL)	2° x 2.5°	Held et al. (2019)
GISS-E2-1-H (NASA-GISS)	2° x 2.5°	Kelley et al. (2020)
HadGEM3-GC3.1-LL (MOHC)	1.25° x 1.875°	Andrews et al. (2020)
IPSL-CM6A-LR (IPSL)	1.3° x 2.5°	Boucher et al. (2020)
MIROC6 (MIROC)	1.4° x 1.4°	Tatebe et al. (2019)
MPI-ESM1-2-LR (MPI-M)	1.9° x 1.9°	Müller et al. (2018)
MRI-ESM2.0 (MRI)	1.1° x 1.1°	Yukimoto et al. (2019)
NorESM2-LM (MRI)	1.9° x 2.5°	Seland et al. (2020)

SI Table 2: List of CMIP6 models used for examining trends in the nearshore hurricane environment for the future period (2015-2100). For each model, a single ensemble member realization under the 'SSP585' emissions scenario is used.

Model (Institution)	**∼Atmospheric resolution (lat x lon)**	**Reference**
ACCESS-CM2 (CSIRO-ARCCSS)	1.25° x 1.875°	Bi et al. (2020)
BCC-CSM2-MR (BCC)	1.1° x 1.1°	Wu et al. (2019)
CESM2 (NCAR)	0.9° x 1.2°	Danabasoglu et al. (2020)
CMCC-CM2-SR5 (CMCC)	0.9° x 1.25°	Cherchi et al. (2019)
CNRM-ESM2-1 (CERFACS)	1.4° x 1.4°	Séférian et al. (2019)
CanESM5 (CCCma)	2.8° x 2.8°	Swart et al. (2019)
E3SM-1-1 (US Dept. of Energy)	1° x 1°	Golaz et al. (2019)
EC-Earth3 (EC-Earth-Consortium)	1.25° x 1.25°	Döscher et al. (2021)
GFDL-CM4 (NOAA-GFDL)	2° x 2.5°	Held et al. (2019)
INM-CM5-0 (INM)	1.5° x 2°	Volodin and Gritsun (2018)
IPSL-CM6A-LR (IPSL)	1.3° x 2.5°	Boucher et al. (2020)
MIROC6 (MIROC)	1.4° x 1.4°	Tatebe et al. (2019)
MPI-ESM1-2-LR (MPI-M)	1.9° x 1.9°	Müller et al. (2018)
MRI-ESM2.0 (MRI)	1.1° x 1.1°	Yukimoto et al. (2019)
UKESM1-0-LL (MOHC)	1.25° x 1.875°	Sellar et al. (2019)

SI Table 3: List of HighResMIP models used for examining changes in nearshore hurricane intensification for the future period. For each model, tracks are obtained from the 'hist-1950' simulation covering the 36-year historical period 1979-2014 and from the 'highres-future' simulation covering the period 2015-2050. For the 'highres-future' simulations, which are a continuation of the 'hist-1950' simulations, the forcing fields are from the 'SSP585' scenario.

Model (Institution)	**∼Atmospheric resolution (lat x lon)**	**Ensembles**	**Reference**
CNRM-CM6-1-HR (CERFACS)	0.5° x 0.5°	1	Voldoire et al. (2019)
EC-Earth3P-HR (EC-Earth-Consortium)	0.35° x 0.35°	2	Haarsma et al. (2020)
HadGEM3-GC31-HH (MOHC)	0.3° x 0.3°	1	Roberts et al. (2019)
HadGEM3-GC31-HM (MOHC)	0.3° x 0.3°	3	Roberts et al. (2019)
MPI-ESM1-2-XR (MPI-M)	0.5° x 0.5°	1	Gutjahr et al. (2019)

References

Andrews, M. B., Ridley, J. K., Wood, R. A., Andrews, T., Blockley, E. W., Booth, B., ... others (2020). Historical simulations with hadgem3-gc3. 1 for cmip6. *Journal of Advances in Modeling Earth Systems*, *12*(6), e2019MS001995.

Bi, D., Dix, M., Marsland, S., O'Farrell, S., Sullivan, A., Bodman, R., ... others (2020). Configuration and spin-up of access-cm2, the new generation australian community climate and earth system simulator coupled model. *Journal of Southern Hemisphere Earth Systems Science*, *70*(1), 225–251.

Boucher, O., Servonnat, J., Albright, A. L., Aumont, O., Balkanski, Y., Bastrikov, V., ... others (2020). Presentation and evaluation of the ipsl-cm6a-lr climate model. *Journal of Advances in Modeling Earth Systems*, *12*(7), e2019MS002010.

Cherchi, A., Fogli, P. G., Lovato, T., Peano, D., Iovino, D., Gualdi, S., ... others (2019). Global mean climate and main patterns of variability in the cmcc-cm2 coupled model. *Journal of Advances in Modeling Earth Systems*, *11*(1), 185–209.

Danabasoglu, G., Lamarque, J.-F., Bacmeister, J., Bailey, D., DuVivier, A., Edwards, J., ... others (2020). The community earth system model version 2 (cesm2). *Journal of Advances in Modeling Earth Systems*, *12*(2), e2019MS001916.

Döscher, R., Acosta, M., Alessandri, A., Anthoni, P., Arneth, A., Arsouze, T., ... others (2021). The ec-earth3 earth system model for the climate model intercomparison project 6. *Geoscientific Model Development Discussions*, 1–90.

Golaz, J.-C., Caldwell, P. M., Van Roekel, L. P., Petersen, M. R., Tang, Q., Wolfe, J. D., ... others (2019). The doe e3sm coupled model version 1: Overview and evaluation at standard

resolution. *Journal of Advances in Modeling Earth Systems*, *11*(7), 2089–2129.

Gutjahr, O., Putrasahan, D., Lohmann, K., Jungclaus, J. H., von Storch, J.-S., Brüggemann, N., ... Stössel, A. (2019). Max planck institute earth system model (mpi-esm1. 2) for the high-resolution model intercomparison project (highresmip). *Geoscientific Model Development*, *12*(7), 3241–3281.

Haarsma, R., Acosta, M., Bakhshi, R., Bretonnière, P.-A., Caron, L.-P., Castrillo, M., ... others (2020). Highresmip versions of ec-earth: Ec-earth3p and ec-earth3p-hr–description, model computational performance and basic validation. *Geoscientific Model Development*, *13*(8), 3507–3527.

Held, I., Guo, H., Adcroft, A., Dunne, J., Horowitz, L., Krasting, J., ... others (2019). Structure and performance of gfdl's cm4. 0 climate model. *Journal of Advances in Modeling Earth Systems*, *11*(11), 3691–3727.

Kelley, M., Schmidt, G. A., Nazarenko, L. S., Bauer, S. E., Ruedy, R., Russell, G. L., ... others (2020). Giss-e2. 1: Configurations and climatology. *Journal of Advances in Modeling Earth Systems*, *12*(8), e2019MS002025.

Müller, W. A., Jungclaus, J. H., Mauritsen, T., Baehr, J., Bittner, M., Budich, R., ... others (2018). A higher-resolution version of the max planck institute earth system model (mpi-esm1. 2-hr). *Journal of Advances in Modeling Earth Systems*, *10*(7), 1383–1413.

Roberts, M. J., Baker, A., Blockley, E. W., Calvert, D., Coward, A., Hewitt, H. T., ... others (2019). Description of the resolution hierarchy of the global coupled hadgem3-gc3. 1 model as used in cmip6 highresmip experiments. *Geoscientific Model Development*, *12*(12), 4999–5028.

Séférian, R., Nabat, P., Michou, M., Saint-Martin, D., Voldoire, A., Colin, J., ... others (2019). Evaluation of cnrm earth system model, cnrm-esm2-1: Role of earth system processes in present-day and future climate. *Journal of Advances in Modeling Earth Systems*, *11*(12), 4182–4227.

Seland, Ø., Bentsen, M., Olivié, D., Toniazzo, T., Gjermundsen, A., Graff, L. S., ... others (2020). Overview of the norwegian earth system model (noresm2) and key climate response of cmip6 deck, historical, and scenario simulations. *Geoscientific Model Development*, *13*(12), 6165–6200.

Sellar, A. A., Jones, C. G., Mulcahy, J. P., Tang, Y., Yool, A., Wiltshire, A., ... others (2019). Ukesm1: Description and evaluation of the uk earth system model. *Journal of Advances in Modeling Earth Systems*, *11*(12), 4513–4558.

Swart, N. C., Cole, J. N., Kharin, V. V., Lazare, M., Scinocca, J. F., Gillett, N. P., ... others (2019). The canadian earth system model version 5 (canesm5. 0.3). *Geoscientific Model Development*, *12*(11), 4823–4873.

Tatebe, H., Ogura, T., Nitta, T., Komuro, Y., Ogochi, K., Takemura, T., ... others (2019). Description and basic evaluation of simulated mean state, internal variability, and climate sensitivity in miroc6. *Geoscientific Model Development*, *12*(7), 2727–2765.

Voldoire, A., Saint-Martin, D., Sénési, S., Decharme, B., Alias, A., Chevallier, M., ... others (2019). Evaluation of cmip6 deck experiments with cnrm-cm6-1. *Journal of Advances in Modeling Earth Systems*, *11*(7), 2177–2213.

Volodin, E., & Gritsun, A. (2018). Simulation of observed climate changes in 1850–2014 with climate model inm-cm5. *Earth System Dynamics*, *9*(4), 1235–1242.

Wu, T., Lu, Y., Fang, Y., Xin, X., Li, L., Li, W., ... others (2019). The beijing climate center climate system model (bcc-csm): the main progress from cmip5 to cmip6. *Geoscientific Model Development*, *12*(4), 1573–1600.

Wu, T., Zhang, F., Zhang, J., Jie, W., Zhang, Y., Wu, F., ... others (2020). Beijing climate center earth system model version 1 (bcc-esm1): model description and evaluation of aerosol simulations. *Geoscientific Model Development*, *13*(3), 977–1005.

Yukimoto, S., Kawai, H., Koshiro, T., Oshima, N., Yoshida, K., Urakawa, S., ... others (2019). The meteorological research institute earth system model version 2.0, mri-esm2. 0: Description and basic evaluation of the physical component. *Journal of the Meteorological Society of Japan. Ser. II*.

Ziehn, T., Chamberlain, M. A., Law, R. M., Lenton, A., Bodman, R. W., Dix, M., ... Srbinovsky, J. (2020). The australian earth system model: Access-esm1. 5. *Journal of Southern Hemisphere Earth Systems Science*, *70*(1), 193–214.